Recurrent exon-deleting activating mutations in *AHR* act as drivers of urinary tract cancer

Judith M. Vlaar[1], Anouska Borgman[2], Eric Kalkhoven[2], Denise Westland[1], Nicolle Besselink[1], Charles Shale[3,4], Bishoy M. Faltas[5], Peter Priestley[3,4], Ewart Kuijk[1,6], Edwin Cuppen[1,3,6,7]

[1] Center for Molecular Medicine and Oncode Institute, University Medical Center Utrecht, the Netherlands.

[2] Center for Molecular Medicine, University Medical Center Utrecht, the Netherlands.

[3] Hartwig Medical Foundation, Amsterdam, The Netherlands.

[4] Hartwig Medical Foundation Australia, Sydney, New South Wales, Australia.

[5] Department of Medicine and Department of Cell and Developmental Biology, Weill Cornell Medicine, New York, NY, United States.

[6] These authors contributed equally to this work: Ewart Kuijk, Edwin Cuppen

[7] contact: e.cuppen@hartwigmedicalfoundation.nl

Competing interests

The authors declare no competing interests.

Abstract

Bladder cancer has a high recurrence rate and low survival of advanced stage patients. Few genetic drivers of bladder cancer have thus far been identified. We performed in-depth structural variant analysis on whole-genome sequencing data of 206 metastasized urinary tract cancers. In ˜10% of the patients, we identified recurrent in-frame deletions of exons 8 and 9 in the aryl hydrocarbon receptor gene (*AHR*$^{\Delta e8\text{-}9}$), which codes for a ligand-activated transcription factor. Pan-cancer analyses show that *AHR*$^{\Delta e8\text{-}9}$ is highly specific to urinary tract cancer and mutually exclusive with other bladder cancer drivers. In *AHR*$^{\Delta e8\text{-}9}$ the ligand-binding domain is disrupted and we show that this results in ligand-independent AHR-pathway activation. In bladder organoids, *AHR*$^{\Delta e8\text{-}9}$ induces a transformed phenotype that is characterized by upregulation of AHR target genes, downregulation of differentiation markers and upregulation of genes associated with stemness and urothelial cancer. Furthermore, *AHR*$\Delta^{e8\text{-}9}$ expression results in anchorage independent growth of bladder organoids, indicating tumorigenic potential. DNA-binding deficient *AHR*$^{\Delta e8\text{-}9}$ fails to induce transformation, suggesting a role for AHR target genes in the acquisition of the oncogenic phenotype. In conclusion, we show that *AHR*$^{\Delta e8\text{-}9}$ is a novel driver of urinary tract cancer and that the AHR pathway could be an interesting therapeutic target.

Introduction

Bladder cancer is the fourth most common cancer in men with a 5-year survival rate of about 77% [1]. Despite risk stratification, the recurrence rate of bladder cancer is high and requires ongoing monitoring and treatment, which makes it also the costliest malignancy out of all cancers [2]. With recent advances, the therapeutic options have been expanded to include immune checkpoint inhibitors and antibody-drug conjugates, while clinical studies for targeted drug approaches are ongoing [3,4]. However, treatment and overall survival of cases with advanced stages of bladder cancer have not really improved in the last decades as compared to other cancers and there remains a need for the identification of drivers of bladder cancer tumorigenesis to effectively target early-stage disease and reduce tumor progression [5,6].

Genomic analyses of bladder cancer of various stages and grades have shown that bladder cancer is a heterogeneous disease of which the high mutation burden is largely driven by activation of APOBEC mutagenesis [7–9]. Molecular characterization revealed activating *FGFR3* alterations in ~16% of patients, with a higher prevalence in non-muscle invasive bladder cancer [9,10]. Furthermore, positive selection of mutated genes in the RTK-Ras-PI3K pathway (such as *FGFR3*, *PIK3CA*, and *ERBB2*), the p53-Rb pathway (such as *TP53*, *RB1*, and *ATM*), and genes involved in chromatin remodeling (*KDM6A* and *KMT2D*) has been identified in biopsies of patients with bladder cancer [7,9].

A recent study identified a rare non-synonymous mutation (Q383H) in *AHR* as an APOBEC-associated hotspot mutation in bladder cancer, suggesting *AHR* as a potential driver of bladder cancer [11]. *AHR* is a ligand activated transcription factor involved in the cellular response to toxic aromatic hydrocarbons as well as cell type and context-specific physiologic functions [12]. Increased *AHR* expression and activity have been associated with poor prognosis and survival for multiple cancers such as breast, lung, and upper urinary tract cancers [13]. However, the relevance and functional consequences of cancer-associated *AHR* mutations in bladder cancer are still poorly understood.

67 Here, we describe the identification of novel recurrent exon-deleting *AHR* alterations
68 in the pan-cancer whole-genome sequencing database of metastatic cancers from Hartwig
69 Medical Foundation. Using state-of-the-art data analysis tools with improved functionality for
70 detecting structural variants we identified a previously unnoticed recurrent in-frame deletion
71 of exons 8 and 9 in *AHR*. Together with the Q383H point mutation and *AHR* gene
72 amplifications, *AHR* variants comprise ~19% of patients with urinary tract cancer. We
73 demonstrate that the recurrent mutations lead to constitutively activated AHR signaling and
74 induces an oncogenic phenotype in bladder cells. Our results suggest that aberrant AHR
75 signaling is an important driver of urothelial tumorigenesis.

Results

AHR is frequently mutated in urinary tract cancers.

To identify genetic factors involved in urinary tract cancers, we analyzed the Hartwig database, which represents whole-genome sequencing data of solid metastatic tumors and normal tissue of 4500 patients [14]. Utilizing improved structural variant detection algorithms [15,16], we detected a novel deletion spanning exons 8 and 9 of the *AHR* gene ($AHR^{\Delta e8\text{-}9}$) in 22 (10.7%) out of the 206 urinary tract samples (Fig. 1a, 1b). The $AHR^{\Delta e8\text{-}9}$ is identified in several urinary tract cancer subtypes, most of which are in bladder cancer (12/22) and pyelum (7/22) (Supplementary table 1). In the complete pan-cancer data set, the $AHR^{\Delta e8\text{-}9}$ mutant is identified in only three non-urinary tract samples. The identified exonic deletion was validated in RNA-sequencing, which was available for 129 out of 206 urinary tract samples. Read support for the AHR exon 7-10 splice junction was identified in all urinary tract samples harboring $AHR^{\Delta e8\text{-}9}$ (n = 16; Supplementary table 1) and confirmed the in-frame loss of exons 8 and 9 for six samples in which the genomic start position of the deletion is located within the coding sequence of exon 8.

The relatively small size of the *AHR* deletion (~ 3kb) may explain why it has not been identified in previous studies [9,17]. Most of the 3' breakpoint junctions are positioned in a narrow window of 30 bp between 2 *Alu* elements (*AluYa5* and *AluY*) and overlap with the 3' site of the *AluYa5* element (Fig. 1a). Such inverted *Alu* repeats have been identified as strong initiators of genetic instability [18]. The high prevalence in urinary tract cancer of such a rare event strongly suggests positive selection. Analysis of an independent RNA-sequencing dataset of urinary tract cancers from Weill Cornell Medicine confirmed the presence of the 7-10 splice junction in 8% (2/24) of samples. One of the bladder cancer samples with the detected splice junction was of primary origin (out of 8 primary tumors in this dataset). Together, these results demonstrate that the $AHR^{\Delta e8\text{-}9}$ is present in primary and metastatic urinary tract cancer (Supplementary table 3).

102 To identify additional events in the *AHR* gene we performed a targeted analysis of
103 the Hartwig database. We identified recurrent gene amplifications and a recurrent point
104 mutation, in 16 (7.8%) and 2 (1.0%) of the urinary tract cancer patients, respectively (Fig. 1a,
105 1b). The c.1149G>C (AHR^{Q383H}) point mutation was previously reported as an APOBEC-
106 associated hotspot mutation in bladder cancer based on the TCGA PanCancer Atlas data [11].
107 The AHR^{Q383H} point mutation was found in 11 patients out of ~11,000 patients in the TCGA
108 PanCancer Atlas, which are mainly of primary tumor origin [19,20]. The majority (n = 8)
109 occurred in bladder urothelial carcinomas with the other three in hepatocellular carcinoma,
110 papillary renal cell carcinoma, and lung adenocarcinoma. Thus, like the $AHR^{\Delta e8\text{-}9}$ variant, the
111 AHR^{Q383H} mutation is highly specific for urinary tract cancer.
112 AHR ligand-activated transcription factor that contains a basic Helix-Loop-Helix/PER-
113 ARNT-SIM (bHLH/PAS) motif. AHR contains two PAS domains of which the PAS-B domain
114 contains the ligand binding domain (LBD) (Fig. 1c) [12,21]. AHR is part of a cytoplasmic protein
115 complex containing HSP90, p23, and XAP2 (Fig. 1d). Upon ligand binding, AHR dissociates
116 from the complex and translocates to the nucleus where it forms a heterodimer with ARNT
117 [22]. The AHR/ARNT complex subsequently binds to Xenobiotic Response Elements (XREs)
118 in the genome to activate the transcription of target genes such as the phase I and II drug
119 metabolizing enzymes CYP1A1 and CYP1B1 [12]. At the protein level, the $AHR^{\Delta e8\text{-}9}$ deletion
120 results in an in-frame protein coding sequence with the loss of 84 amino acids (p. 303-387),
121 disrupting the PAS-B domain and the C-terminal part of the ligand-binding domain of the
122 protein. The HSP90 and XAP2 protein binding domains are predicted to be affected, while
123 the dimerization region of the protein likely remains intact (Fig. 1c).
124 Among the urinary tract cancer patients in the Hartwig database, *AHR* alterations are
125 mutually exclusive with *FGFR3* alterations and *PIK3CA* mutations, although the significance
126 is impacted by low sample numbers (*FGFR3*: Odds ratio = 0.24 p = 0.21, *PIK3CA*: Odds
127 ratio = 0.30 p = 0.32). The tendency of mutual exclusivity with genes from the RTK-Ras-PI3K
128 pathway strengthens the idea that *AHR* is an independent driver of urinary tract cancer, with
129 potential convergence on the RTK-Ras-PI3K pathway. *AHR* alterations do not show

130 depletion with genes involved in chromatin remodeling or the tumor suppressors *TP53* and
131 *Rb1* (Fig. 1e, Supplementary table 4).

132 For tumors with *AHR* amplifications, *AHR* expression is increased compared to the
133 non-amplified urinary tract cancer samples (Fig. 1f). Urinary tract cancers with $AHR^{\Delta e8\text{-}9}$
134 showed increased expression of AHR target genes, which was not observed in the *AHR*
135 amplified or *AHR* non-affected samples (Fig. 1g). No RNA sequencing data was available for
136 the 2 patients with the AHR^{Q383H} mutation.

137 The $hAHR^{Q383H}$ mutation affects ligand binding affinity and specificity

138 The mouse ortholog of AHR^{Q383H} (Ahr^{Q377}) can form hydrogen bonds with Ahr ligands in the
139 ligand-binding domain and mutations that change this residue affect ligand binding affinities
140 [23–25]. To examine if ligand binding affinities are also affected for the human AHR (hAHR), we
141 measured the transcriptional activity of $hAHR^{Q383H}$ and $hAHR^{WT}$ in an XRE-luciferase reporter
142 assay. Both the $hAHR^{WT}$ and $hAHR^{Q383H}$ expressing cells showed strong transcriptional
143 activity with AHR ligands TCDD and B[a]P (Fig. 2a). Stimulation with B[a]P resulted in a
144 higher induction of luciferase transcription for the $hAHR^{Q383H}$ mutant than for the $hAHR^{WT}$,
145 suggesting a difference in ligand affinity between both variants. The AHR antagonist CH-
146 223191 reduced transcriptional activation in $hAHR^{WT}$ cells stimulated with TCDD or B[a]P
147 (Fig. 2a) [26,27]. Surprisingly, incubation of $hAHR^{Q383H}$ with CH-223191 resulted in
148 transcriptional activation and no antagonism was observed when CH-223191 was combined
149 with TCDD or B[a]P (Fig. 2a). To examine this altered ligand-binding specificity, we analyzed
150 protein localization in RPE1 cells. In the absence of exogenous ligands, both $hAHR^{Q383H}$ and
151 $hAHR^{WT}$ proteins are mainly localized to the cytoplasm and both proteins show nuclear
152 translocation upon incubation with TCDD or B[a]P (Fig. 2b, Supplementary fig. 1). Incubation
153 with the antagonist CH-223191 also resulted in nuclear translocation of $hAHR^{Q383H}$, while the
154 $hAHR^{WT}$ remains localized to the cytoplasm (Fig. 2b). The difference in responses between
155 the $hAHR^{Q383H}$ and $hAHR^{WT}$ to AHR agonists and antagonists demonstrates the Q383H
156 mutant is more sensitive to AHR pathway stimulation.

157 The hAHR$^{\Delta e8\text{-}9}$ mutant leads to constitutive AHR pathway activation

158 To study the functional consequences of *AHR*$^{\Delta e8\text{-}9}$, we created transgenic *hAHR*$^{\Delta e8\text{-}9}$ RPE1
159 cells and mouse bladder organoids. In contrast with *hAHR*^{WT}, the *hAHR*$^{\Delta e8\text{-}9}$ protein is
160 localized in the nucleus regardless of the presence or absence of a ligand (Fig. 2b).
161 Expression of the *hAHR* mutants in mouse bladder organoids confirmed constitutive nuclear
162 localization of the hAHR$^{\Delta e8\text{-}9}$ mutant (Fig. 2c). In XRE-luciferase reporter assays, the degree
163 of transcriptional activation by hAHR$^{\Delta e8\text{-}9}$ was similar for all the conditions, irrespective of the
164 presence of AHR ligands. Moreover, the AHR antagonist CH-223191 did not affect the
165 transcriptional activation activity of hAHR$^{\Delta e8\text{-}9}$ (Fig. 2a). Increased concentrations of *hAHR*^{WT}
166 and *hAHR*$^{\Delta e8\text{-}9}$ constructs in the transfections resulting in increased expression levels and
167 revealed that hAHR$^{\Delta e8\text{-}9}$ induces higher transcriptional activity levels than hAHR^{WT} in
168 untreated conditions (Fig. 2d).

169 To further characterize the consequences of the constitutive nuclear localization of
170 hAHR$^{\Delta e8\text{-}9}$ we performed bulk RNA-sequencing on mouse bladder organoids expressing
171 *hAHR*$^{\Delta e8\text{-}9}$ or *hAHR*^{WT} in the presence or absence of TCDD. Untreated *hAHR*$^{\Delta e8\text{-}9}$ organoids
172 differentially expressed several genes compared to the *hAHR*^{WT} organoids, including the
173 AHR target genes *Cyp1a1*, *Cyp1b1*, *Ahrr*, *Gsta1*, and *Tiparp* demonstrating constitutive
174 activation of the AHR pathway (Fig. 3a, b). The expression pattern of up and down regulated
175 genes is similar for *hAHR*$^{\Delta e8\text{-}9}$ in untreated and TCDD treated conditions, confirming that loss
176 of exons 8 and 9 leads to ligand-independent activation of the AHR pathway, which is in line
177 with the upregulation of these genes in *AHR*$^{\Delta e8\text{-}9}$ positive urinary tract cancers (Fig. 1g).
178 Thus, *AHR*$^{\Delta e8\text{-}9}$ leads to constitutive activation of the AHR pathway.

179 The *hAHR*^{WT} organoids treated with TCDD also show upregulation of the canonical
180 AHR target genes, but do not show the same downregulated genes (Fig. 3a). This
181 observation indicates a different effect on the transcriptome between the constitutively active
182 hAHR$^{\Delta e8\text{-}9}$ and the 24h TCDD stimulated hAHR^{WT} condition. Moreover, overexpression of
183 *hAHR*^{WT} and *hAHR*^{Q383H} without the addition of exogenous ligands already results in modest
184 pathway activation when compared with control organoids that are not transgenic for *hAHR*

185 (Fig. 3b). These observations are in line with the higher induction of luciferase transcription
186 in the untreated condition for the *hAHR*^{WT} and *hAHR*^{Q383H} constructs compared to the control
187 in the luciferase assay (Fig. 2a).

188 The *hAHR*$^{\Delta e8\text{-}9}$ mutant induces cellular transformation

189 The bladder is a stratified epithelium, with stem cells that reside in the basal cell layer that
190 support organ regeneration and renewal. Upon differentiation, the stem cells give rise to
191 intermediate cells and luminal umbrella cells [28]. Mouse bladder organoids enriched for
192 undifferentiated cells have a reduced diameter of the lumen and increased thickness of the
193 epithelial layer when compared to organoids composed of differentiated cells [29]. We
194 observed a mixture of cystic and compact organoids in the mouse bladder organoids
195 expressing *hAHR*^{WT}, indicating a heterogeneous population of differentiated and
196 undifferentiated cells. No cystic organoids were observed in the organoids expressing
197 *hAHR*$^{\Delta e8\text{-}9}$ indicating a more basal stem-cell like phenotype (Fig. 3c).

198 We performed GO enrichment analysis on all differentially expressed genes in RNA-
199 sequencing data of the mouse organoids to understand which processes are affected by
200 *hAHR*$^{\Delta e8\text{-}9}$. Most outstanding is the downregulation of genes related to the extracellular
201 matrix and cell periphery organization (Fig. 3d, Supplementary table 5). Moreover, *hAHR*$^{\Delta e8\text{-}9}$
202 expressing mouse organoids show downregulation of the differentiation markers *Upk3a*,
203 *Upk1a*, and *Krt18* and upregulation of the stem cell markers *Wnt5a*, and *Krt1* when
204 compared to *hAHR*^{WT} organoids (Fig. 3e) [29–31]. Together, these observations indicate that
205 *hAHR*$^{\Delta e8\text{-}9}$ promotes a basal stem-cell like phenotype in bladder cells.

206 Because RNA-seq was performed on bulk cultures, the transcriptional changes
207 induced by *hAHR*$^{\Delta e8\text{-}9}$ may reflect a shift in the composition of the cell types towards a more
208 homogeneous population, or the transformation of cells towards a novel phenotype. To
209 discriminate between these scenarios, we performed scRNA-seq on the mouse bladder
210 organoid lines. Dimensional reduction and unsupervised clustering revealed the presence of
211 7 clusters (Fig. 4a). Based on the genes enriched in the different clusters, cluster 0

212 represents a basal phenotype (characterized by *Krt14*, *Trp63*, *Bcam* and *Agrn*), cluster 1
213 represents an intermediate/luminal phenotype (characterized by *Krt19*, *Krt18*, *Upk1b*, *Cldn4*,
214 *Cldn7, Ceacam1* and *Alcam*), and clusters 3 and 5 represent cells that are in the S-phase
215 and M-phase of the cell cycle, respectively (Fig. 4a, 4b, Supplementary table 6). Together,
216 these clusters represent a classical stem cell system where stem cells divide to give rise to
217 new stem cells or to cells that differentiate. The vast majority of all cells of the control lines
218 fall into these clusters and in cluster 4, which we were not able to link to a particular cellular
219 phenotype. Strikingly, two clusters (clusters 2 and 6) were almost exclusively occupied by
220 mouse bladder cells expressing $hAHR^{\Delta e8\text{-}9}$ (Fig. 4a, 4c). In addition to the canonical AHR
221 target genes such as *Cyp1b1* and *Tiparp*, cluster 2 expresses basal stem cell markers such
222 as *Krt17*, *Wnt5a*, *Itga6*, *Wnt4* [29]. In addition cluster 2 is characterized by genes that are
223 associated with urothelial cancer, such as: *Htra1* [32], *Cyb5r1* [33], *Steap1* [33,34], *Ptgs2* [35,36], and
224 *Trib3* [37] (Fig. 4b). Cells in cluster 6 show upregulation of *Dsp*, *Pkp1*, *Ppl*, *Jup* and *Krt13*,
225 which are involved in desmosome and intermediate filament cytoskeleton organization. This
226 cluster has some overlap with markers expressed in the luminal-intermediate cluster (cluster
227 1) of the control cells, but with less apparent expression of the umbrella cell markers. This
228 indicates that the cells in cluster 6 represent an intermediate cell type that however fails to
229 differentiate towards luminal umbrella cells. Thus, the constitutive activation of the AHR
230 pathway by $hAHR^{\Delta e8\text{-}9}$ leads to a transformation of cells towards a less differentiated
231 phenotype and the activation of genes linked to urothelial cancer.

232 Cells of a DNA binding deficient variant of the oncogenic $hAHR^{\Delta e8\text{-}9}$ ($hAHR^{\Delta e8\text{-}9DBD}$)
233 clustered among cells of the other control lines and apart from $hAHR^{\Delta e8\text{-}9}$ cells (Fig. 4a). This
234 shows that the cellular transformation of the $hAHR^{\Delta e8\text{-}9}$ organoids depends on the
235 transcriptional activation caused by AHR and is not the result of potential transcription-
236 independent effects caused by the deletion. To functionally explore if the transformed
237 phenotype is accompanied by oncogenic properties, a soft agar growth assay was
238 performed. A higher number of colonies were counted for $hAHR^{\Delta e8\text{-}9}$ organoids compared to

239 *hAHR*^{WT} organoids or control organoids demonstrating that *hAHR*$^{\Delta e8\text{-}9}$ confers anchorage-
240 independent growth to bladder cells (Fig. 4d).
241 Together, these observations demonstrate that transcriptional changes driven by the
242 constitutively active *hAHR*$^{\Delta e8\text{-}9}$ lead to a transformation of cells towards a cancerous
243 phenotype that fails to differentiate and is able to grow independent of anchorage to the
244 extracellular matrix.

245 Discussion

246 In this study, we show high prevalence of *AHR* alterations in urinary tract cancers and
247 provide functional validations to support that these aberrations are oncogenic and drive
248 urinary tract cancer. These findings are in line with mouse studies that have shown that *AHR*
249 overexpression or pathway activation can lead to malignant transformation of epithelial cells
250 [38–40]. A variety of molecular signaling pathways have been previously linked to AHR-
251 mediated tumorigenesis whether or not in a cancer type-specific background and/or driven
252 by AHR agonists [13,41]. This includes the biotransformation of hydrocarbons by CYP enzymes
253 to mutagenic intermediates which can induce DNA adducts, cross-talk of AHR with other
254 signaling pathways, and interaction of AHR with other binding partners than ARNT to
255 promote transcription of non-canonical genes [42–47]. However, the underlying molecular
256 signaling pathways driving the tumorigenesis of urinary tract cancers in patients with
257 activating mutations in *AHR* remains unclear. The tendency of mutual exclusivity between
258 *AHR*, *FGFR3*, and *PIK3CA* alterations may indicate convergence on the same pathway,
259 although a fully independent parallel oncogenic pathway in bladder cancer driven by *AHR*
260 cannot be excluded. The *hAHR*^{Q383H} and *hAHR*$^{\Delta e8\text{-}9}$ variants are almost uniquely detected in
261 urothelial cancers, which suggests this tissue is particularly sensitive to deregulated *AHR*
262 signaling. However, our results, nor information in literature, provides clues why AHR
263 activation is so specific for bladder cancer, so this will require further investigations.
264 We demonstrate that the *hAHR*^{Q383H} mutation leads to increased sensitivity which
265 may also lead to overactivity of the AHR pathway in the urinary tract, thereby driving

266 tumorigenesis. This likely also holds true for *AHR* amplifications since overexpression of
267 *hAHR*^{wt} in different models shows a modest increase of AHR pathway activation compared
268 to the controls. It is not known if the ligands that induce overactive AHR signaling in the
269 tumors with *AHR* amplified and *AHR*^{Q383H} backgrounds are of environmental origin (like
270 components in tobacco smoke) or have an endogenous source (like metabolites) [48].
271 Surprisingly, we observed *hAHR*^{Q383H} activation upon treatment with the AHR antagonist CH-
272 223191. This contrasts with a recent study that demonstrated reduced viability upon
273 treatment with CH-223191 of the bladder cancer cell line KMBC2 harboring the *AHR*^{Q383H}
274 mutation [11]. A possible explanation for the apparent discrepancy in results may lie in the
275 different types of experiments that were conducted. The reduced viability of the KMBC2 cell
276 line after CH-223191 incubation may also be independent of alterations in AHR pathway
277 activity.

278 Patients that harbor *AHR* activating mutations could potentially benefit from AHR
279 targeted therapies [49]. Here we show that the mode of action of AHR activation differs
280 between the different mutations, which implies that tailored therapies depending on the
281 underlying mutational event are required. Most classic AHR antagonists function by
282 interference with the ligand-binding domain, but this domain is not targetable for the AHR$^{\Delta e8\text{-}9}$
283 mutant as this domain is deleted. Therefore, functional screens to identify specific AHR$^{\Delta e8\text{-}9}$
284 targeting compounds or the identification of essential downstream activated processes could
285 be a next step towards the identification of novel treatment strategies for selected urinary
286 tract cancer patients in the context of precision medicine.

287 ## Material and Methods

288 ### Driver gene status urinary tract cohort

289 Variant detection and driver likelihood status are based on the Hartwig database [14]. Driver
290 likelihood is introduced to select for a sample specific likelihood of each gene based on the
291 type of variant and taking mutation load per sample into account. To select for affected
292 genes in the urinary tract cancer samples, the driver likelihood score is set to >0.8 and
293 detected gene fusions with a high impact are included. Visualized are the genes affected in
294 more than 12.5% of the samples (top 12 genes). Mutually exclusivity is pairwise calculated
295 with Fisher Exact Test based on Odd Ratio cut-offs as described in Gao et al. [19].
296

297 ### Gene constructs

298 A plasmid containing the *hAHR*^{WT} sequence was purchased from Origene (RC209832). The
299 Q383H point mutation was introduced with site-directed mutagenesis with forward primer
300 cattgtaactcacagaccactaacagatg and reverse primer gttagtggtctgtgagttacaatgatataatc. The
301 *hAHR*^{WT}, *hAHR*^{Q383H}, and *hAHR*$^{\Delta e8\text{-}9}$ sequences were cloned in a lentiviral plasmid (Addgene
302 #52961) and subsequently to pcDNA3.1 vector with the In-fusion HD Eco-dry cloning
303 (Takarabio). Primers for lentiviral plasmid are: forward N-flag
304 caggaccggttctaggatatcgccaccatggattacaaagacgatgacgataagaacagcagcagcgccaac, forward
305 caggaccggttctaggatatcgccaccatgaacagcagcagcgcc, reverse
306 ttgttgcgccggatcgcaggaatccactggatgtcaaatcag, reverse C-flag
307 ttgttgcgccggatcgcttatcgtcatcgtctttgtaatccaggaatccactggatgtcaaatcag, forward deletion
308 tggttgtgatgccaaagatgaggaaggaacagagca and reverse deletion
309 gttccttcctcatctttggcatcacaaccaatagg. Primers cloning of *AHR* sequences to pcDNA3.1 vector
310 are forward taccgagctcggatcatatcgccaccatgaacag and reverse
311 gatatctgcagaattttacaggaatccactggatgtcaaat. For the DNA binding deficient variant of *AHR*$^{\Delta 8\text{-}}$
312 ^{9}, mutations were introduced to substitute the amino acids Histidine 39 and Arginine 40 with
313 Alanines [50].

314 The luciferase reporter vector pGL3-XRE-Luc2 reporter vector was constructed using
315 an in-house pGL3-minP-Luc2 vector containing DNA binding sequence
316 “gggaggtacttggagcggc” with primers forward-1
317 gcgtgctagcccgggTTGCGTGACCctcgagatctgcgat, reverse-1
318 atcgcagatctcgagGGTCACGCAAcccgggctagcacgc, forward-2
319 aatcgataaggatccTTGCGTGACCgtcgaccgatgccct, reverse-2
320 agggcatcggtcgacGGTCACGCAAggatccttatcgatt.
321

322 Cell culture

323 All cells were cultured in a humidified atmosphere at 37°C under 5%CO_2 and 20%O_2.
324 Lentivirus particles containing *hAHR* constructs were produced by transient calcium
325 phosphate transfection of HEK293T. Virus particles were concentrated with Lenti-X
326 Concentrator (Takarabio) according to the manufacturer’s directions. Mouse bladder
327 organoids were a kind gift from drs Hans Clevers and Jasper Mullenders and were cultured
328 as previously reported[51]. In short, mouse bladder organoids were plated in droplets of ice-
329 cold Matrigel (Corning). After the matrigel had solidified, a complete mouse bladder medium
330 was added consisting of Advanced DMEM/F-12 supplemented with HEPES, Glutamax, 1%
331 penicillin, 1% streptomycin, Nicotinamide (10 mM), N-Acetylcysteine (1.25 mM), FGF10 (100
332 ng/mL of Peprotech 100-26), FGF7 (25 ng/mL of Peprotech 100-19), A83-01 (500 nM), B27
333 (ThermoFisher 17504001) and primocin (Invivogen). Organoids were split weekly either
334 through mechanical shearing with a pulled Pasteur’s pipet or by dissociation using TrypLE.
335 To increase survival the medium was supplemented with ROCK inhibitor (Y-27632, 10 μM)
336 after splitting.
337 RPE1 and HEK293T cells were cultured in DMEM, 10% fetal bovine serum, 1%
338 penicillin, and 1% streptomycin. After transduction, RPE1 cells and the mouse bladder
339 organoids were placed on 10-15 μg/ml and 1 μg/ml puromycin selection, respectively. Cells

340 were incubated with 10 nM TCDD (LGC), 10 μM B[a]P (sigma), or 10 μM CH-223191
341 (Sanbio) or vehicle alone (DMSO) for 24h unless otherwise stated.

342 Immunofluorescence

343 RPE1 cells expressing *hAHR* mutants were plated on coverslips and incubated with TCDD,
344 B[a]P, CH-223191 or untreated (DMSO) for 4 or 24h. Cells were fixed in 4% formaldehyde,
345 permeabilized with 0.3% Triton X-100 in PBS, and blocked with 4% BSA in PBS. AHR was
346 stained with Anti-AHR antibody (Abcam ab190797) in blocking buffer. After incubation with
347 the primary antibody, cells were washed followed by incubation with secondary antibodies
348 conjugated with Alexa fluor dyes. Subsequently, the cells were washed, counterstained with
349 DAPI, and mounted on microscope slides. Images were taken with predefined settings on
350 Zeiss LSM510 microscope and analyzed with Fuij/imageJ. Ratios of AHR signal intensities
351 were calculated by determining average grey value intensities for each nucleus, based on
352 dapi staining, and for each corresponding cytoplasm, as 1μM band around each nucleus.
353 The first steps in the immunofluorescence procedure for the mouse bladder
354 organoids are different from the procedure described previously. First, dispase was added to
355 a final concentration of 1mg/ml to a warm medium and incubated for 30 min at 37°C to
356 dissolve the Matrigel. Organoids were harvested by gentle pipetting, collected in a tube, and
357 washed with cold Advanced DMEM/F12. The organoids were centrifuged, washed in PBS
358 followed by another centrifugation step. The resulting organoid pellet was resuspended in
359 100μl PBS and transferred to Lab-Tek Chamber slides. The organoids were fixed by the
360 addition of 4% formaldehyde followed by 1h incubation at RT. The organoids attached to the
361 bottom of the chamber slide were washed twice with PBS. Subsequently, the organoids
362 were incubated in blocking buffer and the immunofluorescence procedure was followed as
363 described for the RPE1 cells.

364 Luciferase reporter gene assay

365 HEK293T cells were cultured in 24-wells plates and transiently transfected with pcDNA3.1
366 empty vector or pcDNA3.1 vector containing the expression cassette of $hAHR^{WT}$, $hAHR^{Q383H}$,

367 or *hAHR*$^{\Delta e8\text{-}9}$ (10 ng), together with the pGL3-XRE-Luc2 reporter vector (1000 ng) and pRL-
368 CMV Renilla vector (2 ng). 24h after transfection, cells were treated with ligand TCDD (50
369 nM) or B[a]P and/or antagonist CH223191 for approximately 24h. Luciferase activity was
370 measured with the Dual-Luciferase reporter assay system and normalized for Renilla activity
371 (Promega, Madison, WI). The results are averages of at least three independent
372 experiments assayed in duplicate ± SEM. Results are presented as change relative to the
373 empty vector in the untreated (DMSO) condition.

374 RNA-sequencing

375 The RNA from the transgenic mouse bladder organoids was isolated with Trizol
376 (ThermoFisher) according to the manufacturer's instructions. RNA-seq libraries were
377 prepared using TruSeq Stranded Total RNA Library Prep Kit (Illumina) according to the
378 manufacturer's protocol. RNA-seq libraries were pooled and sequenced on a NextSeq2000
379 (Illumina) in 1x50bp single end mode. RNA sequencing reads were aligned against mouse
380 reference genome GRCm38 using STAR and the number of reads mapping to genes was
381 counted using featureCounts all by using a custom in-house pipeline
382 (https://github.com/UMCUGenetics/RNASeq-NF). The Bioconductor package DESeq2 was
383 used to normalize raw read counts and to perform differential gene expression analysis with
384 apeglm shrinkage [52,53]. The analyses were performed with significant (P.adjust<0.05) and
385 differentially expressed (Log2FoldChange>2.5) genes with exception of luminal and basal
386 marker analyses where smaller differences were included (Log2FoldChange>1.5). The
387 Bioconductor package clusterProfiler and Revigo were used for GO enrichment analysis
388 [54,55].
389

390 scRNA-seq

391 The transgenic mouse bladder organoids were cultured in 2D and dissociated to single cells
392 using a 10 min incubation with TryLE. Cells were sorted into 384-well capture plates and the
393 scRNA library preparation and sequencing were performed according to the SORT-seq

394 protocol by Single Cell Discoveries B.V. [56]. For all single cells, reads were aligned to the
395 mouse reference genome GRCm38 and Sort-seq read counts were filtered to exclude reads
396 with identical library-, cell- and molecules [56]. With the Seurat R package, low quality cells
397 were removed by a cut-off of 10000 transcripts per cell and the data was normalized and
398 scaled [57]. The top 2000 most variable genes in the dataset were identified and used for
399 principal component analysis to determine dimensionality and clustering of the dataset.
400 Cluster gene markers were detected using a Wilcoxon rank sum test between each cluster
401 and the rest of the cells in the dataset with a bonferroni correction for multiple testing.

402 Soft agar assay

403 3% agarose (REF11388991001) was dissolved and autoclaved in 100 ml EBSS. One
404 volume of melted 3% agarose was mixed with four volumes of Advanced DMEM/F12 to
405 obtain a 0.6% solution. This mixture was added to 6-well plates (1.5 ml/well) in which the
406 gels were allowed to solidify. Subsequently, Tryple was used to prepare single-cell
407 suspensions of the mouse bladder organoids. The cells were counted and for each
408 condition, 2.5 ml of cell suspension was prepared at a concentration of $1x10^{e4}$ cells/ml in
409 complete medium. The cell suspension was mixed 1:1 with a warm 0.6% agarose solution to
410 get 0.5 $x10^{e4}$ cells/ml in 0.3% agarose solution. Per well 1.5 ml agarose/cell mixture was
411 plated. The next day 300 µl of the medium was added and the cells were refed every 2-4
412 days. After 3 weeks the cells were stained with nitroblue tetrazolium chloride solution and
413 pictures were made. Colonies were counted using ImageJ.

414 Acknowledgments

415 We are grateful to Jasper Mullenders and Hans Clevers for providing the mouse bladder
416 organoids. We thank Livio Kleij for his support with microscopy, Single Cell Discoveries for
417 support with single cell RNA sequencing, the Utrecht Sequencing Facility for providing
418 sequencing service, and the UMC Utrecht Bioinformatics Expertise Core for data analysis
419 and data handling. The Utrecht Sequencing Facility is subsidized by the University Medical
420 Center Utrecht, Hubrecht Institute, Utrecht University, and The Netherlands X-omics

Initiative (NWO project 184.034.019). The UMC Utrecht Bioinformatics Expertise Core is subsidized by the University Medical Center Utrecht, Center for Molecular Medicine. This publication and the underlying study have been made possible partly based on the data that Hartwig Medical Foundation and the Center of Personalised Cancer Treatment (CPCT) have made available to the study.

Data availability

The bulk RNA-sequencing and the scRNA-seq data of the mouse bladder organoids have been deposited in ENA with the accession code PRJEB49233.

Author contributions

JMV, E Kuijk, NB, DW and EC designed and performed experiments including data analysis and interpretation. AB, and E Kalkhoven designed and performed the luciferase assay experiments. CS and PP conducted Hartwig database analysis. BMF provided Weill Cornell Medicine data analysis. PP and EC conceived the original idea. EC and E Kuijk supervised the project. JMV, E Kuijk, and EC wrote the manuscript with input from all authors.

Competing interests

The authors declare no competing interests.

439 References

440 1 American Cancer Society. Cancer Facts & Figures 2020. Atlanta: American Cancer
441 Society; 2020.

442 2 James AC, Gore JL. The costs of non-muscle invasive bladder cancer. *Urol Clin North*
443 *Am* 2013; **40**: 261–269.

444 3 Lenis AT, Lec PM, Chamie K, Mshs MD. Bladder Cancer: A Review. *JAMA* 2020; **324**:
445 1980–1991.

446 4 Loriot Y, Necchi A, Park SH, Garcia-Donas J, Huddart R, Burgess E *et al.* Erdafitinib in
447 Locally Advanced or Metastatic Urothelial Carcinoma. *N Engl J Med* 2019; **381**: 338–
448 348.

449 5 Berdik C. Unlocking bladder cancer. *Nature* 2017; **551**: S34–S35.

450 6 Abdollah F, Gandaglia G, Thuret R, Schmitges J, Tian Z, Jeldres C *et al.* Incidence,
451 survival and mortality rates of stage-specific bladder cancer in United States: a trend
452 analysis. *Cancer Epidemiol* 2013; **37**: 219–225.

453 7 Lawson ARJ, Abascal F, Coorens THH, Hooks Y, O'Neill L, Latimer C *et al.* Extensive
454 heterogeneity in somatic mutation and selection in the human bladder. *Science* 2020;
455 **370**: 75–82.

456 8 Nakauma-González, J. Alberto, J. Alberto Nakauma-González, Maud Rijnders, Job van
457 Riet, Michiel S. van der Heijden, Jens Voortman, Edwin Cuppen, et al. 2021. "Molecular
458 Characterization Reveals Genomic and Transcriptomic Subtypes of Metastatic
459 Urothelial Carcinoma." bioRxiv 2021.03.17.435757.

460 9 Robertson AG, Kim J, Al-Ahmadie H, Bellmunt J, Guo G, Cherniack AD *et al.*
461 Comprehensive Molecular Characterization of Muscle-Invasive Bladder Cancer. *Cell*
462 2018; **174**: 1033.

463 10 Cancer Genome Atlas Research Network. Comprehensive molecular characterization of
464 urothelial bladder carcinoma. *Nature* 2014; **507**: 315–322.

465 11 Shi M-J, Meng X-Y, Fontugne J, Chen C-L, Radvanyi F, Bernard-Pierrot I. Identification
466 of new driver and passenger mutations within APOBEC-induced hotspot mutations in
467 bladder cancer. *Genome Med* 2020; **12**: 85.

468 12 Denison MS, Soshilov AA, He G, DeGroot DE, Zhao B. Exactly the same but different:
469 promiscuity and diversity in the molecular mechanisms of action of the aryl hydrocarbon
470 (dioxin) receptor. *Toxicol Sci* 2011; **124**: 1–22.

471 13 Wang Z, Snyder M, Kenison JE, Yang K, Lara B, Lydell E *et al.* How the AHR Became
472 Important in Cancer: The Role of Chronically Active AHR in Cancer Aggression. *Int J*
473 *Mol Sci* 2020; **22**. doi:10.3390/ijms22010387.

474 14 Priestley P, Baber J, Lolkema MP, Steeghs N, de Bruijn E, Shale C *et al.* Pan-cancer
475 whole-genome analyses of metastatic solid tumours. *Nature* 2019; **575**: 210–216.

476 15 Shale, Charles, Jonathan Baber, Daniel L. Cameron, Marie Wong, Mark J. Cowley,
477 Anthony T. Papenfuss, Edwin Cuppen, and Peter Priestley. 2020. "Unscrambling
478 Cancer Genomes via Integrated Analysis of Structural Variation and Copy Number."

479 BioRxiv 2020.12.03.410860.

480 16 Cameron DL, Baber J, Shale C, Valle-Inclan JE, Besselink N, van Hoeck A *et al.*
481 GRIDSS2: comprehensive characterisation of somatic structural variation using single
482 breakend variants and structural variant phasing. *Genome Biol* 2021; **22**: 202.

483 17 ICGC/TCGA Pan-Cancer Analysis of Whole Genomes Consortium. Pan-cancer analysis
484 of whole genomes. *Nature* 2020; **578**: 82–93.

485 18 Lobachev KS, Stenger JE, Kozyreva OG, Jurka J, Gordenin DA, Resnick MA. Inverted
486 Alu repeats unstable in yeast are excluded from the human genome. *EMBO J* 2000; **19**:
487 3822–3830.

488 19 Gao J, Aksoy BA, Dogrusoz U, Dresdner G, Gross B, Sumer SO *et al.* Integrative
489 analysis of complex cancer genomics and clinical profiles using the cBioPortal. *Sci*
490 *Signal* 2013; **6**: l1.

491 20 Cerami E, Gao J, Dogrusoz U, Gross BE, Sumer SO, Aksoy BA *et al.* The cBio cancer
492 genomics portal: an open platform for exploring multidimensional cancer genomics data.
493 *Cancer Discov* 2012; **2**: 401–404.

494 21 Larigot L, Juricek L, Dairou J, Coumoul X. AhR signaling pathways and regulatory
495 functions. *Biochim Open* 2018; **7**: 1–9.

496 22 Seok S-H, Lee W, Jiang L, Molugu K, Zheng A, Li Y *et al.* Structural hierarchy
497 controlling dimerization and target DNA recognition in the AHR transcriptional complex.
498 *Proc Natl Acad Sci U S A* 2017; **114**: 5431–5436.

499 23 Xing Y, Nukaya M, Satyshur KA, Jiang L, Stanevich V, Korkmaz EN *et al.* Identification
500 of the Ah-receptor structural determinants for ligand preferences. *Toxicol Sci* 2012; **129**:
501 86–97.

502 24 Pandini A, Denison MS, Song Y, Soshilov AA, Bonati L. Structural and functional
503 characterization of the aryl hydrocarbon receptor ligand binding domain by homology
504 modeling and mutational analysis. *Biochemistry* 2007; **46**: 696–708.

505 25 Bisson WH, Koch DC, O'Donnell EF, Khalil SM, Kerkvliet NI, Tanguay RL *et al.*
506 Modeling of the Aryl Hydrocarbon Receptor (AhR) Ligand Binding Domain and Its Utility
507 in Virtual Ligand Screening to Predict New AhR Ligands. Journal of Medicinal
508 Chemistry. 2009; **52**: 5635–5641.

509 26 Kim S-H, Henry EC, Kim D-K, Kim Y-H, Shin KJ, Han MS *et al.* Novel Compound 2-
510 Methyl-2H-pyrazole-3-carboxylic Acid (2-methyl-4-o-tolylazo-phenyl)-amide (CH-
511 223191) Prevents 2,3,7,8-TCDD-Induced Toxicity by Antagonizing the Aryl Hydrocarbon
512 Receptor. Molecular Pharmacology. 2006; **69**: 1871–1878.

513 27 Zhao B, DeGroot DE, Hayashi A, He G, Denison MS. CH223191 Is a Ligand-Selective
514 Antagonist of the Ah (Dioxin) Receptor. Toxicological Sciences. 2010; **117**: 393–403.

515 28 Yamany T, Van Batavia J, Mendelsohn C. Formation and regeneration of the
516 urothelium. *Curr Opin Organ Transplant* 2014; **19**: 323–330.

517 29 Santos CP, Lapi E, Martínez de Villarreal J, Álvaro-Espinosa L, Fernández-Barral A,
518 Barbáchano A *et al.* Urothelial organoids originating from Cd49f mouse stem cells
519 display Notch-dependent differentiation capacity. *Nat Commun* 2019; **10**: 4407.

520 30 Yu Z, Liao J, Chen Y, Zou C, Zhang H, Cheng J *et al.* Single-Cell Transcriptomic Map of

521 the Human and Mouse Bladders. *J Am Soc Nephrol* 2019; **30**: 2159–2176.

522 31 Guo CC, Bondaruk J, Yao H, Wang Z, Zhang L, Lee S *et al.* Assessment of Luminal and
523 Basal Phenotypes in Bladder Cancer. *Sci Rep* 2020; **10**: 9743.

524 32 Lorenzi T, Lorenzi M, Altobelli E, Marzioni D, Mensà E, Quaranta A *et al.* HtrA1 in
525 human urothelial bladder cancer: A secreted protein and a potential novel biomarker.
526 International Journal of Cancer. 2013. doi:10.1002/ijc.28280.

527 33 Stroggilos R, Mokou M, Latosinska A, Makridakis M, Lygirou V, Mavrogeorgis E *et al.*
528 Proteome-based classification of Nonmuscle Invasive Bladder Cancer. *Int J Cancer*
529 2020; **146**: 281–294.

530 34 Azumi M, Kobayashi H, Aoki N, Sato K, Kimura S, Kakizaki H *et al.* Six-transmembrane
531 epithelial antigen of the prostate as an immunotherapeutic target for renal cell and
532 bladder cancer. *J Urol* 2010; **183**: 2036–2044.

533 35 Wild PJ, Kunz-Schughart LA, Stoehr R, Burger M, Blaszyk H, Simon R *et al.* High-
534 throughput tissue microarray analysis of COX2 expression in urinary bladder cancer. *Int*
535 *J Oncol* 2005; **27**: 385–391.

536 36 Agrawal U, Kumari N, Vasudeva P, Mohanty NK, Saxena S. Overexpression of COX2
537 indicates poor survival in urothelial bladder cancer. *Ann Diagn Pathol* 2018; **34**: 50–55.

538 37 Yang J, Lin J, An J, Zhao Y, Jing S, Yu M *et al.* TRIB3 Promotes the Malignant
539 Progression of Bladder Cancer: An Integrated Analysis of Bioinformatics and in vitro
540 Experiments. Frontiers in Genetics. 2021; **12**. doi:10.3389/fgene.2021.649208.

541 38 Brooks J, Eltom SE. Malignant transformation of mammary epithelial cells by ectopic
542 overexpression of the aryl hydrocarbon receptor. *Curr Cancer Drug Targets* 2011; **11**:
543 654–669.

544 39 Andersson P, McGuire J, Rubio C, Gradin K, Whitelaw ML, Pettersson S *et al.* A
545 constitutively active dioxin/aryl hydrocarbon receptor induces stomach tumors. *Proc Natl*
546 *Acad Sci U S A* 2002; **99**: 9990–9995.

547 40 Dantsuka A, Ichii O, Hanberg A, Elewa YHA, Otsuka-Kanazawa S, Nakamura T *et al.*
548 Histopathological features of the proper gastric glands in FVB/N-background mice
549 carrying constitutively-active aryl-hydrocarbon receptor. *BMC Gastroenterol* 2019; **19**:
550 102.

551 41 Dietrich C, Kaina B. The aryl hydrocarbon receptor (AhR) in the regulation of cell-cell
552 contact and tumor growth. *Carcinogenesis* 2010; **31**: 1319–1328.

553 42 Shimizu Y, Nakatsuru Y, Ichinose M, Takahashi Y, Kume H, Mimura J *et al.*
554 Benzo[a]pyrene carcinogenicity is lost in mice lacking the aryl hydrocarbon receptor.
555 *Proc Natl Acad Sci U S A* 2000; **97**: 779–782.

556 43 Wilson SR, Joshi AD, Elferink CJ. The tumor suppressor Kruppel-like factor 6 is a novel
557 aryl hydrocarbon receptor DNA binding partner. *J Pharmacol Exp Ther* 2013; **345**: 419–
558 429.

559 44 Vogel CFA, Li W, Wu D, Miller JK, Sweeney C, Lazennec G *et al.* Interaction of aryl
560 hydrocarbon receptor and NF-κB subunit RelB in breast cancer is associated with
561 interleukin-8 overexpression. *Arch Biochem Biophys* 2011; **512**: 78–86.

562 45 Xie G, Peng Z, Raufman J-P. Src-mediated aryl hydrocarbon and epidermal growth

563 factor receptor cross talk stimulates colon cancer cell proliferation. American Journal of
564 Physiology-Gastrointestinal and Liver Physiology. 2012; **302**: G1006–G1015.

565 46 Fritsche E, Schäfer C, Calles C, Bernsmann T, Bernshausen T, Wurm M *et al.*
566 Lightening up the UV response by identification of the arylhydrocarbon receptor as a
567 cytoplasmatic target for ultraviolet B radiation. *Proc Natl Acad Sci U S A* 2007; **104**:
568 8851–8856.

569 47 Baker JR, Sakoff JA, McCluskey A. The aryl hydrocarbon receptor (AhR) as a breast
570 cancer drug target. *Med Res Rev* 2020; **40**: 972–1001.

571 48 Denison MS, Nagy SR. Activation of the aryl hydrocarbon receptor by structurally
572 diverse exogenous and endogenous chemicals. *Annu Rev Pharmacol Toxicol* 2003; **43**:
573 309–334.

574 49 Kolluri SK, Jin U-H, Safe S. Role of the aryl hydrocarbon receptor in carcinogenesis and
575 potential as an anti-cancer drug target. *Arch Toxicol* 2017; **91**: 2497–2513.

576 50 Dong L, Ma Q, Whitlock JP. DNA Binding by the Heterodimeric Ah Receptor. Journal of
577 Biological Chemistry. 1996; **271**: 7942–7948.

578 51 Mullenders J, de Jongh E, Brousali A, Roosen M, Blom JPA, Begthel H *et al.* Mouse
579 and human urothelial cancer organoids: A tool for bladder cancer research. *Proc Natl*
580 *Acad Sci U S A* 2019; **116**: 4567–4574.

581 52 Love MI, Huber W, Anders S. Moderated estimation of fold change and dispersion for
582 RNA-seq data with DESeq2. *Genome Biol* 2014; **15**: 550.

583 53 Zhu A, Ibrahim JG, Love MI. Heavy-tailed prior distributions for sequence count data:
584 removing the noise and preserving large differences. *Bioinformatics* 2019; **35**: 2084–
585 2092.

586 54 Yu G, Wang L-G, Han Y, He Q-Y. clusterProfiler: an R Package for Comparing
587 Biological Themes Among Gene Clusters. OMICS: A Journal of Integrative Biology.
588 2012; **16**: 284–287.

589 55 Supek F, Bošnjak M, Škunca N, Šmuc T. REVIGO summarizes and visualizes long lists
590 of gene ontology terms. *PLoS One* 2011; **6**: e21800.

591 56 Muraro MJ, Dharmadhikari G, Grün D, Groen N, Dielen T, Jansen E *et al.* A Single-Cell
592 Transcriptome Atlas of the Human Pancreas. *Cell Syst* 2016; **3**: 385–394.e3.

593 57 Hao Y, Hao S, Andersen-Nissen E, Mauck WM 3rd, Zheng S, Butler A *et al.* Integrated
594 analysis of multimodal single-cell data. *Cell* 2021; **184**: 3573–3587.e29.

595

596 Figures Legends

597 Figure 1. *AHR* alterations in somatic metastatic urinary tract patients.

598 a. Schematic representation of *AHR* gene (ENST00000242057.4 - GRCh37) with a
599 magnification of the genomic region around exon 7 - 9 (Chr7:17372389-17378532). The
600 point mutation *Q383H* (c.1149G>C) is marked with an asterisk. The black bars in the lower
601 part of the figure represent the extent of the genomic deletions identified in the urinary tract
602 cancer patients. See supplementary table 2 for genomic positions of the deletions. b. Pie
603 chart of the number of detected *AHR* alterations: *AHR* amplification (Amp), $AHR^{\Delta e8\text{-}9}$,
604 AHR^{Q383H} or non-affected samples in the urinary tract patient cohort of the Hartwig database.
605 c. Schematic illustration of the AHhR functional domains and the positions of AHR^{Q383H} and
606 $AHR^{\Delta e8\text{-}9}$. The deletion ($AHR^{\Delta e8\text{-}9}$) disrupts the PAS-B domain, ligand-binding domain (LBD),
607 and XAP2 and HSP90 protein interaction domains. d. Canonical AHhR signaling pathway.
608 (Figure created with BioRender.com). e. Visualization of top 12 affected genes per mutation
609 type in urinary tract cancer samples of the Hartwig database [14]. Gene names are colored for
610 oncogenes (red) and tumor suppressor genes (blue). f. Boxplot of the adjusted TPM values
611 for *AHR* transcript. Asterisks indicate two samples that contain the deletion ($AHR^{\Delta e8\text{-}9}$) but
612 also have an amplification of the *AHR* gene. g. Boxplot of the adjusted TPM values of AHR
613 target genes.

614

615 Figure 2. Altered protein localization and mediated transcription activation of *hAHR* mutants.
616 a. Luciferase reporter assay of HEK293T cells transfected with empty control, $hAHR^{WT}$,
617 $hAHR^{Q383H}$, or $hAHR^{\Delta e8\text{-}9}$ vectors together with XRE-luciferase reporter construct. Assays
618 were performed with different AHR ligands (TCDD and B[a]P) and AHR antagonist (CH-
619 223191) conditions. Significance was calculated with Student's T-test for stimulated versus
620 untreated condition per construct. * $p < 0.05$, ** $p < 0.01$. RLU = relative luciferase unit. b.
621 Immunofluorescence of RPE1 cells that express $hAHR^{WT}$, $hAHR^{Q383H}$, or $hAHR^{\Delta e8\text{-}9}$ that were
622 incubated for 4h with TCDD or CH-223191. AHR was detected with immunofluorescence
623 (red) and DNA with Dapi (blue). The boxplots present the AHR signal ratio of nuclear to

624 cytoplasmic signal for all individual captured cells. Untransduced cells served as negative
625 controls (left panels). c. Immunofluorescence of mouse bladder organoids that express
626 $hAHR^{WT}$, $hAHR^{Q383H}$, or $hAHR^{\Delta e8\text{-}9}$ and were incubated for 24h with TCDD. AHR was
627 detected with immunofluorescence (red) and DNA with Dapi (blue). d. Luciferase reporter
628 assay of HEK293T cells transfected with increasing concentration of $hAHR^{WT}$, $hAHR^{\Delta e8\text{-}9}$,
629 and empty control vectors.
630
631 Figure 3: Transcriptome analysis of constitutively activated $hAHR^{\Delta e8\text{-}9}$ mutant.
632 a. Rlog values of the 172 most differentially expressed genes between the $hAHR^{WT}$ and
633 $hAHR^{\Delta e8\text{-}9}$ expressing mouse bladder organoids in untreated and TCDD treated conditions.
634 b. Boxplot of normalized counts of RNA reads of AHR target genes for the untreated mouse
635 bladder organoids expressing *hAHR* mutants (n=4). c. Images of Dapi stained mouse
636 bladder organoids expressing *hAHR* mutants. The lower panel shows the magnification of
637 the boxed area. Scale bar 250 µm. d. GO enrichment analysis of $hAHR^{\Delta e8\text{-}9}$ mutant for the
638 cellular component domain. e. Rlog values of basal and luminal cell layer makers for
639 $hAHR^{\Delta e8\text{-}9}$ and $hAHR^{WT}$ expressing mouse bladder organoids.
640
641 Figure 4: Transformed phenotype of $hAHR^{\Delta e8\text{-}9}$ mutant.
642 a. tSNE plot of single cell transcriptomics depicting clusters of the transgenic mouse bladder
643 organoids cells. Plot is coloured for detected clusters and for the different transgenic mouse
644 bladder organoid lines. b. Heatmap depicting expression of selected markers, which are
645 identified by expression analysis, representative for the different identified clusters. c.
646 Contribution of percentage of cells to the different clusters for each transgenic mouse
647 bladder organoid line. d. Soft agar assay of mouse bladder organoids expressing hAHR
648 mutants. Results are presented as the mean ± SD of triplicate samples.
649

650 Supplementary information

651 Supplementary table 1: Overview urinary tract cancer sample data from Hartwig database

652

653 Supplementary table 2: Overview $AHR^{\Delta e8-9}$ breakpoint information

654

655 Supplementary table 3: AHR RNA-sequencing splice junction detection in urinary tract

656 cancer patients from Weill Cornell Medicine

657

658 Supplementary table 4: Driver gene status in urinary tract cancer samples based on Hartwig

659 database.

660

661 Supplementary table 5: GO enrichment analysis details of mouse bladder organoids

662 expressing $hAHR^{\Delta e8-9}$

663

664 Supplementary table 6: Gene markers per cluster in scRNA-seq data of the mouse bladder

665 organoids

666

667 Supplementary figure 1: AHR protein localization after incubation with B[a]P or CH-223191.

668 Immunofluorescence of RPE1 cells that express $hAHR^{WT}$, $hAHR^{Q383H}$, or $hAHR^{\Delta e8-9}$ that were

669 incubated for 4h with B[a]P or with AHR antagonist CH-223191. AHR was detected with

670 immunofluorescence (red) and DNA with Dapi (blue). The boxplots present the AHR signal

671 ratio of nuclear to cytoplasmic signal for all individual captured cells. Untransduced cells

672 served as negative controls (left panels).

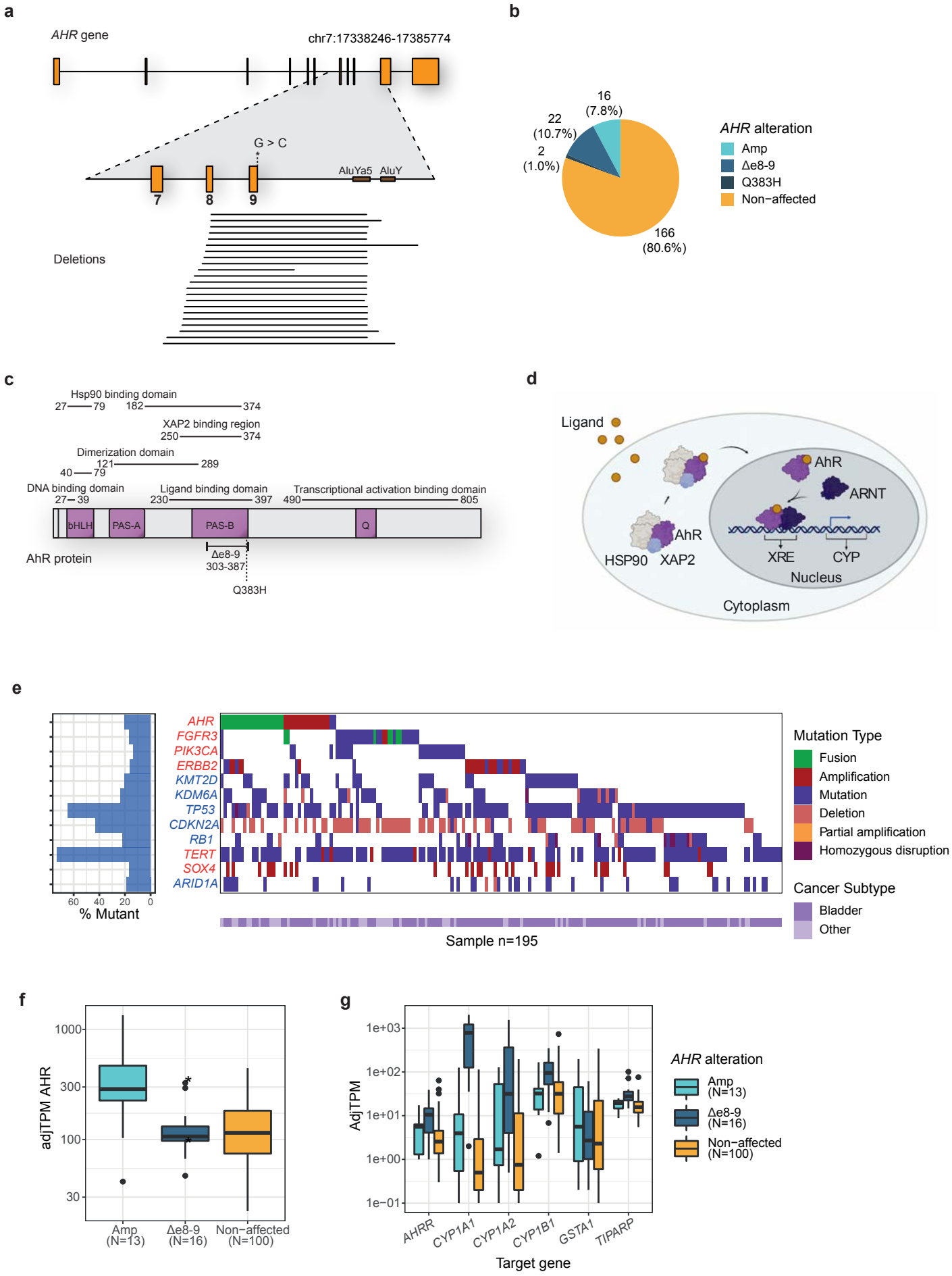
a
AHR gene
chr7:17338246-17385774
G > C
AluYa5
AluY
7
8
9
Deletions
b
16
(7.8%)
22
(10.7%)
2
(1.0%)
166
(80.6%)
AHR alteration
Amp
Δe8-9
Q383H
Non−affected
c
Hsp90 binding domain
27 79 182 374
XAP2 binding region
250 374
Dimerization domain
121 289
40 79
DNA binding domain
27 39
Ligand binding domain
230 397
Transcriptional activation binding domain
490 805
bHLH
PAS-A
PAS-B
Q
AhR protein
Δe8-9
303-387
Q383H
d
Ligand
AhR
ARNT
AhR
HSP90
XAP2
XRE
CYP
Nucleus
Cytoplasm
e
AHR
FGFR3
PIK3CA
ERBB2
KMT2D
KDM6A
TP53
CDKN2A
RB1
TERT
SOX4
ARID1A
60 40 20 0
% Mutant
Sample n=195
Mutation Type
Fusion
Amplification
Mutation
Deletion
Partial amplification
Homozygous disruption
Cancer Subtype
Bladder
Other
f
1000
300
100
30
adjTPM AHR
Amp
(N=13)
Δe8-9
(N=16)
Non−affected
(N=100)
g
1e+03
1e+02
1e+01
1e+00
1e−01
AdjTPM
AHRR
CYP1A1
CYP1A2
CYP1B1
GSTA1
TIPARP
Target gene
AHR alteration
Amp
(N=13)
Δe8-9
(N=16)
Non−affected
(N=100)

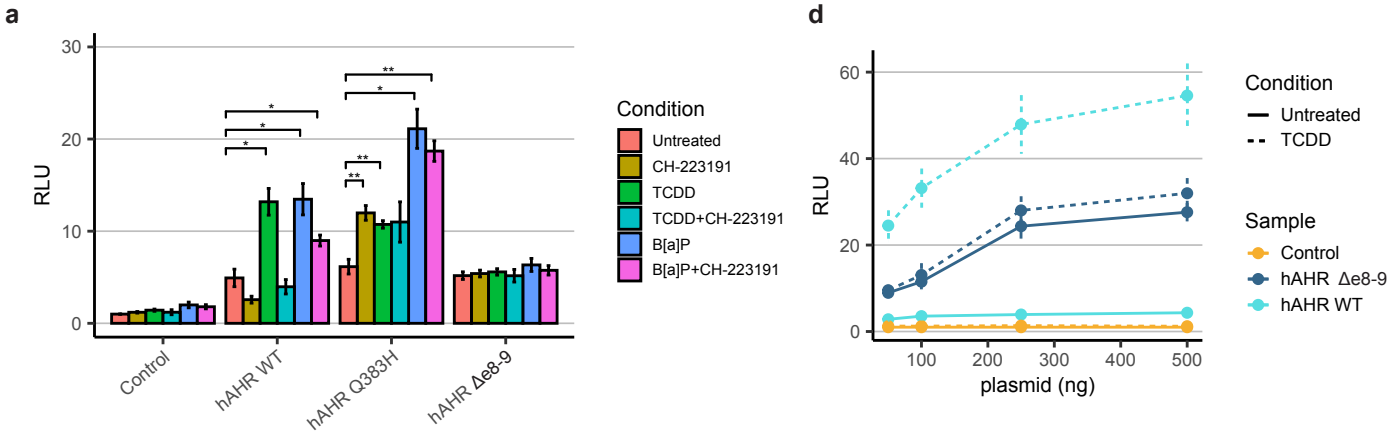
a
RLU
30
20
10
0
Control
hAHR WT
hAHR Q383H
hAHR Δe8-9
Condition
Untreated
CH-223191
TCDD
TCDD+CH-223191
B[a]P
B[a]P+CH-223191
d
RLU
60
40
20
0
100
200
300
400
500
plasmid (ng)
Condition
Untreated
TCDD
Sample
Control
hAHR Δe8-9
hAHR WT

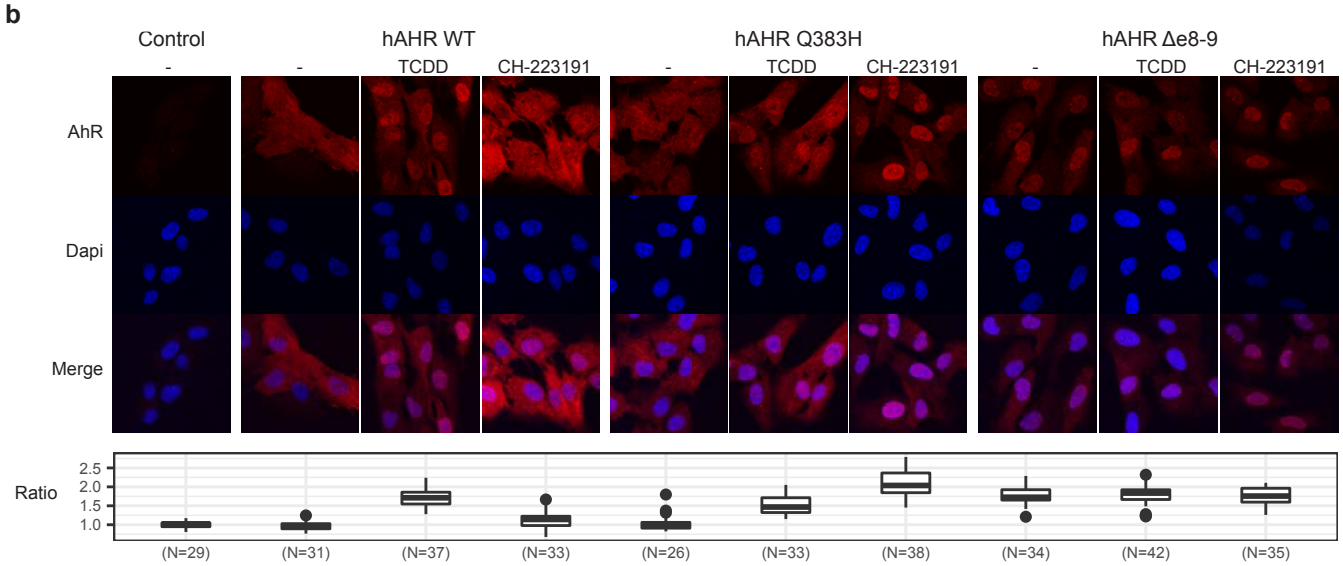
b
Control
hAHR WT
hAHR Q383H
hAHR Δe8-9
-
-
TCDD
CH-223191
-
TCDD
CH-223191
-
TCDD
CH-223191
AhR
Dapi
Merge
Ratio
2.5
2.0
1.5
1.0
(N=29)
(N=31)
(N=37)
(N=33)
(N=26)
(N=33)
(N=38)
(N=34)
(N=42)
(N=35)

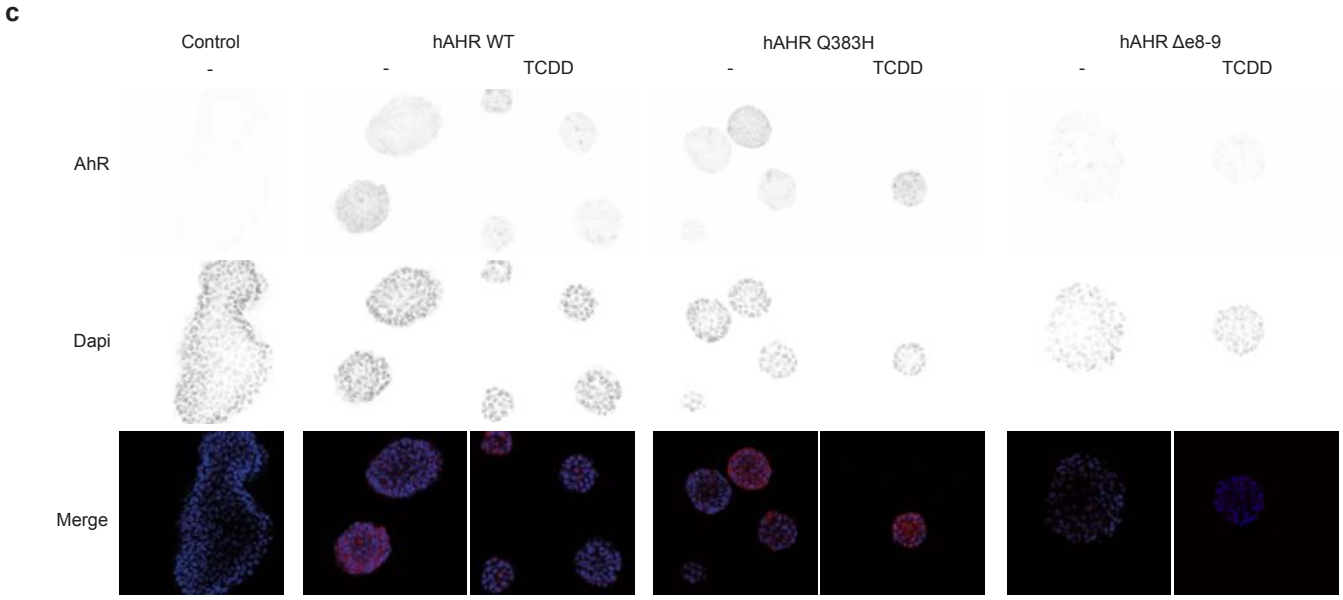
c
Control
hAHR WT
hAHR Q383H
hAHR Δe8-9
-
-
TCDD
-
TCDD
-
TCDD
AhR
Dapi
Merge

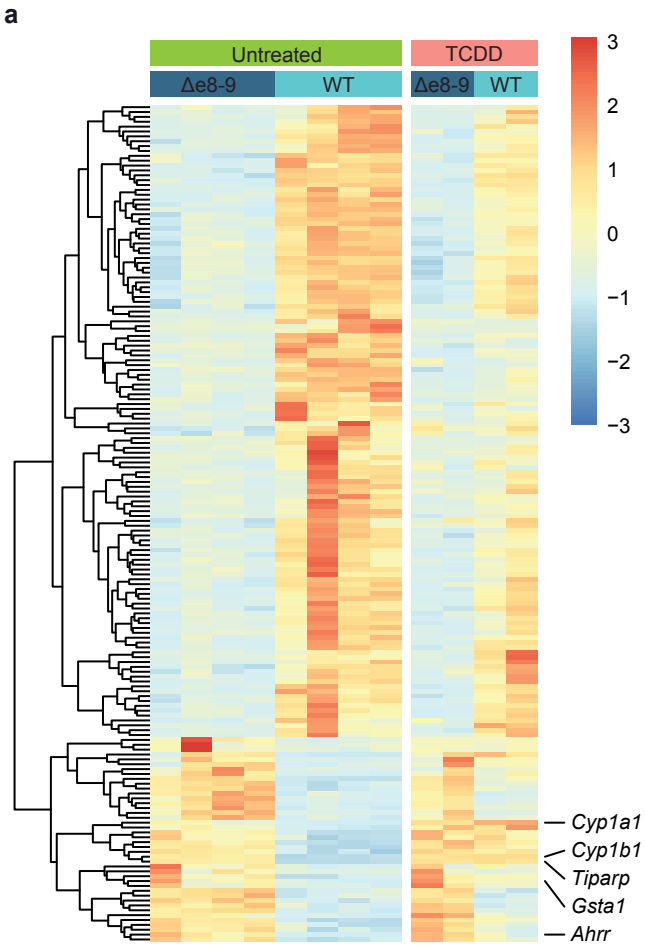
a
Untreated
TCDD
Δe8-9
WT
Δe8-9
WT
3
2
1
0
−1
−2
−3
Cyp1a1
Cyp1b1
Tiparp
Gsta1
Ahrr

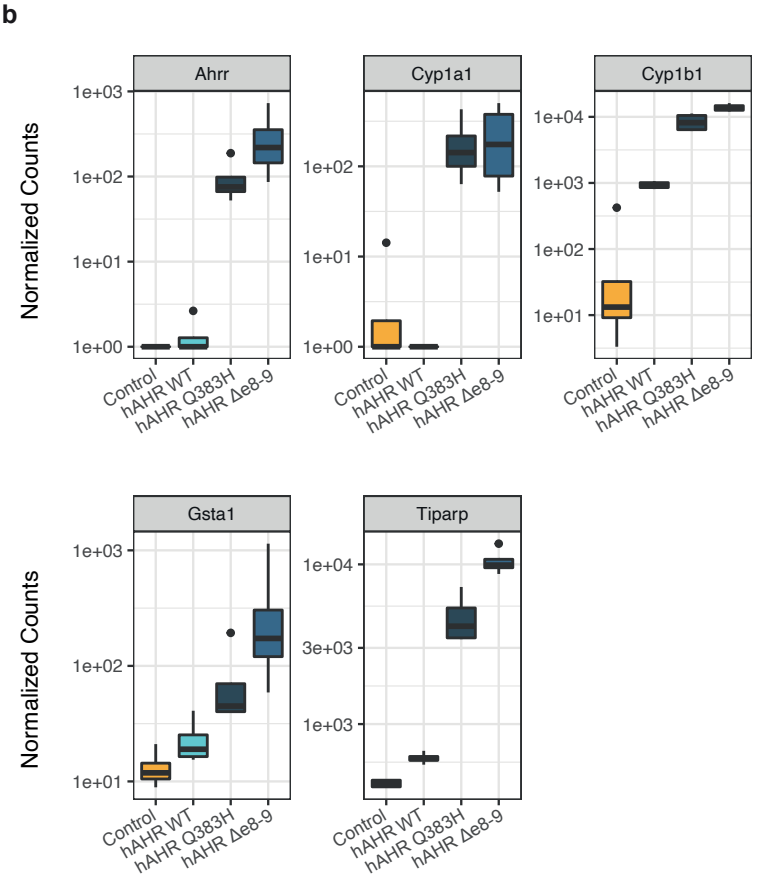
b
Ahrr
Cyp1a1
Cyp1b1
Gsta1
Tiparp
Normalized Counts
Control
hAHR WT
hAHR Q383H
hAHR Δe8-9

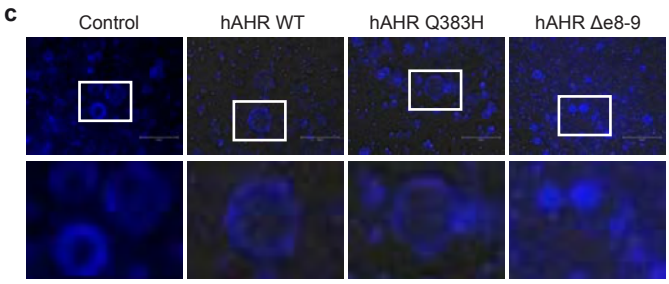
c
Control
hAHR WT
hAHR Q383H
hAHR Δe8-9

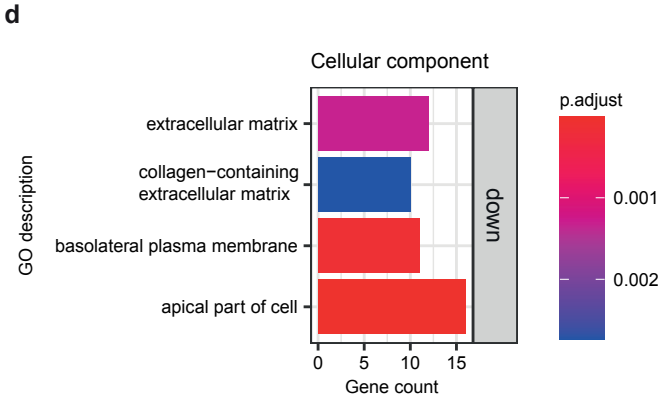
d
Cellular component
GO description
extracellular matrix
collagen−containing extracellular matrix
basolateral plasma membrane
apical part of cell
down
Gene count
p.adjust
0.001
0.002

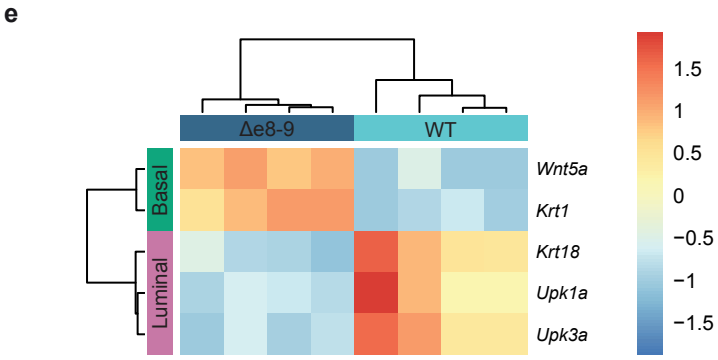
e
Δe8-9
WT
Basal
Luminal
Wnt5a
Krt1
Krt18
Upk1a
Upk3a
1.5
1
0.5
0
−0.5
−1
−1.5

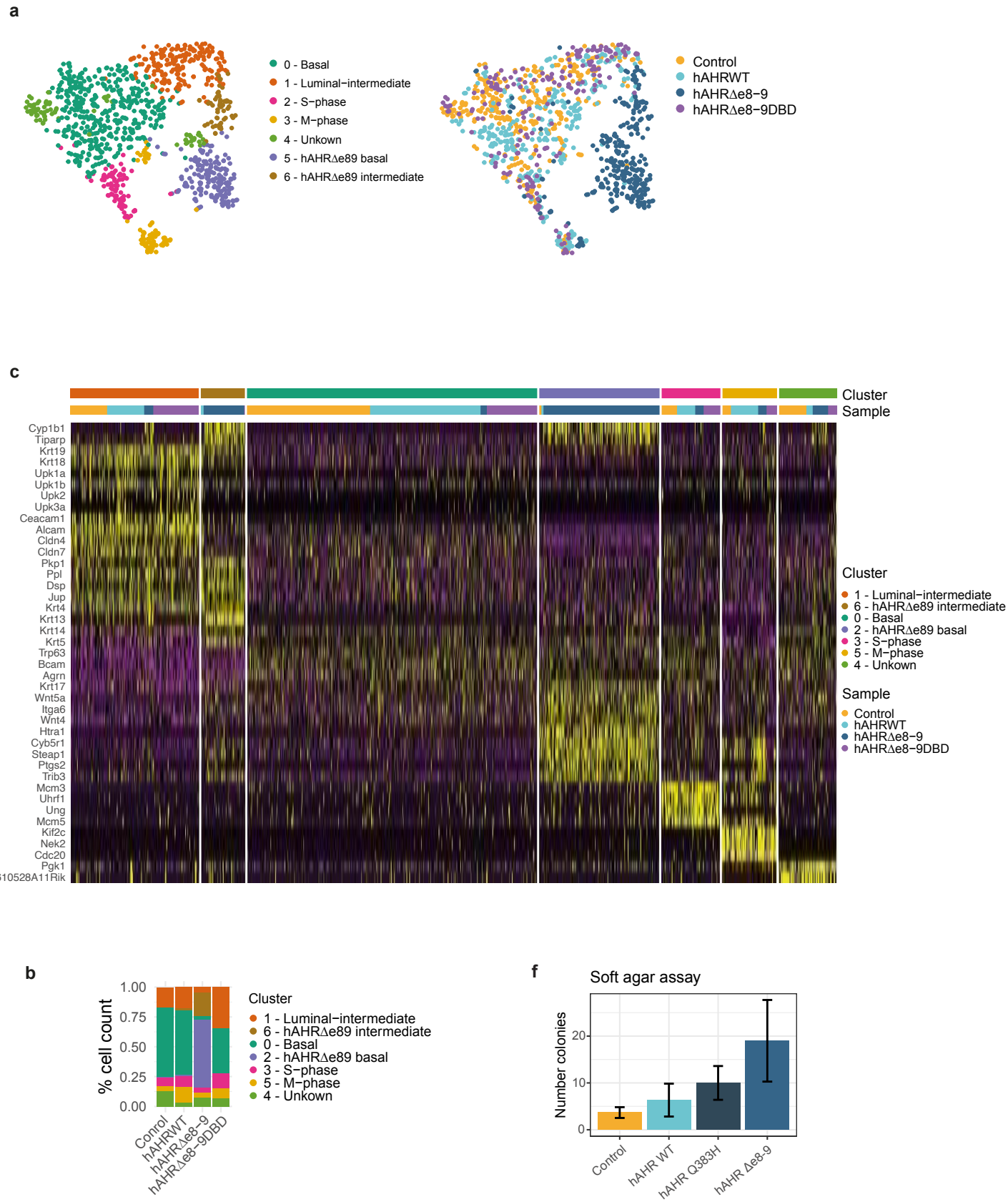
a
0 - Basal
1 - Luminal−intermediate
2 - S−phase
3 - M−phase
4 - Unkown
5 - hAHRΔe89 basal
6 - hAHRΔe89 intermediate
Control
hAHRWT
hAHRΔe8−9
hAHRΔe8−9DBD
c
Cluster
Sample
Cyp1b1
Tiparp
Krt19
Krt18
Upk1a
Upk1b
Upk2
Upk3a
Ceacam1
Alcam
Cldn4
Cldn7
Pkp1
Ppl
Dsp
Jup
Krt4
Krt13
Krt14
Krt5
Trp63
Bcam
Agrn
Krt17
Wnt5a
Itga6
Wnt4
Htra1
Cyb5r1
Steap1
Ptgs2
Trib3
Mcm3
Uhrf1
Ung
Mcm5
Kif2c
Nek2
Cdc20
Pgk1
2610528A11Rik
Cluster
1 - Luminal−intermediate
6 - hAHRΔe89 intermediate
0 - Basal
2 - hAHRΔe89 basal
3 - S−phase
5 - M−phase
4 - Unkown
Sample
Control
hAHRWT
hAHRΔe8−9
hAHRΔe8−9DBD
b
% cell count
1.00
0.75
0.50
0.25
0.00
Conrol
hAHRWT
hAHRΔe8−9
hAHRΔe8−9DBD
Cluster
1 - Luminal−intermediate
6 - hAHRΔe89 intermediate
0 - Basal
2 - hAHRΔe89 basal
3 - S−phase
5 - M−phase
4 - Unkown
f
Soft agar assay
Number colonies
20
10
0
Control
hAHR WT
hAHR Q383H
hAHR Δe8-9